Article

Three Dimensional Pulse Coupled Neural Network Based on Hybrid Optimization Algorithm for Oil Pollution Image Segmentation

Heming Jia [ID], **Zhikai Xing and Wenlong Song** *

College of Mechanical and Electrical Engineering, Northeast Forestry University, Harbin 150040, China;
jiaheming@nefu.edu.cn (H.J.); kai230606@nefu.edu.cn (Z.X.)
* Correspondence: swl@nefu.edu.cn

check for
updates

Abstract: This paper proposes a three dimensional pulse coupled neural network (3DPCNN) image segmentation method based on a hybrid seagull optimization algorithm (HSOA) to solve the oil pollution image. The image of oil pollution is taken by the unmanned aerial vehicle (UAV) in the oil field area. The UAV is good at shooting the ground area, but its ability to identify the oil pollution area is poor. In order to solve this problem, a 3DPCNN-HSOA algorithm is proposed to segment the oil pollution image, and the oil pollution area is segmented to identify the dirty oil area and improve the inspection of environmental pollution. The 3DPCNN image segmentation method has simple structure and good segmentation effect, but it has many parameters and poor segmentation effect for complex oil images. Therefore, we apply HSOA algorithm to optimize the parameters of 3DPCNN algorithm, so as to improve the segmentation accuracy and solve the segmentation of oil pollution images. The experimental results show that the 3DPCNN-HSOA model can separate the oil pollution area from the complex background.

Keywords: oil pollution image segmentation; 3DPCNN; seagull optimization algorithm; thermal exchange optimization

1. Introduction

The pollution of oil pollution to the environment is becoming more and more serious, the Nereids project aims to strengthen civil protection and marine pollution preparedness and cooperation among Greece and Cyprus [1,2]. This project has a good effect on protecting the environment. Fingas, Merv reviewed the remote-sensing of oil spills [3]. This paper analyzed the camera, laser fluorescence sensor, radar detection and other detection means to detect oil spills. T. M. Alves combined the oil spill model with bathymetric, meteorological, oceanographic, and geomorphic data to model a series of oil spills in the eastern Mediterranean [4]. Alves Tiago M. proposed new mathematical and geological models to mitigate potential oil spills in the eastern Mediterranean [5]. Oil spills are serious on the environment, so the monitoring of oil spills are important [6,7]. Now people use video detection [8], UAV [9] and satellites [10] to detect the ground area. The UAV is widely used because of their low cost and flexibility. However, the application of UAV can only record the area or detect it by human observation screen, and the identical effect of the oil pollution area is poor. In order to solve this problem, researchers use image segmentation method to segment the detected image to obtain the oil pollution area and better detect the environment [11,12]. Color image segmentation has always been the focus of many scholars, because color images have rich color space, which brings great challenges to the image segmentation algorithm. There are primarily four types of segmentation methods: thresholding [13–15], boundary-based [16–18], region-based [19,20], and hybrid techniques [21,22].

With the development of artificial neural network, more and more attention has been paid to PCNN model. It has the characteristics of global cooling and synchronous pulse, which makes it widely use in the field of image processing. PCNN, originated from Eckhorn et al. [23] who focus on the study of the synchronous oscillation phenomenon in the visual cortex of cats, has been applied in a variety of applications in image processing [24].

PCNN has broad applications in many aspects for image segmentation [25]. Xiang R proposed a simplified pulse-coupled neural network, which developed based on the comentropy gradient for segmentation of tomato plant images captured at night [26]. The proposed algorithm exhibited the optimal segmentation performance, with the best rate of 91.67%. Chen Y proposed method performs color image segmentation by a simplified pulse-coupled neural network (SPCNN) for the object model image and test image, and then conducted a region-based matching between them [27]. SPCNN could well solve the problem of image segmentation, but due to the large number of parameters in the PCNN model, it was unable to adapt to the segmentation of different images. In order to solve the problem of PCNN with improper parameter selection and determination of circulation iterations which leaded to the image owe-segmentation or over-segmentation, Li H used an Iterative Self-organizing Data Clustering (ISODC) to resolve the problems of the PCNN parameter selection. Experimental results show that the proposed method improves the segmentation speed and achieves good segmentation results [28]. He presented an improved PCNN model that integrated the simplified framework and spectral residual to alleviate the fairly complex determination of parameter problem [29]. The method has high precision of the infrared pedestrian image. Lian J proposed a parameter-adaptive pulse-coupled neural network, which has a low computational complexity for different kinds of medical images and has a high segmentation precision [30]. So, parameter selection of PCNN model plays an important role in image segmentation accuracy.

In order to solve the difficulty of parameter value assignment increases with higher performance, most researchers study how to use an optimization algorithm to solve PCNN parameters. Gao H Y proposed Quantum Geese Swarm Optimization (QGSO) evolve parameters of PCNN, experiment results show that the proposed method can obtain better segmented images and has an excellent performance [31]. Bai W proposed a method of dividing the insulator image based on the simplified model of PCNN is proposed to extract the number of insulator sheds of a string. The method used the PSO algorithm to select the optimal PCNN parameter to realize the binary segmentation of the insulator image [32]. Due to the differences in actual engineering problems that various meta-heuristics adapt to solve, the traditional optimization methods are often not satisfactory in computational accuracy. Therefore, the selection of optimization algorithm becomes particularly important for PCNN model parameters. There are many kinds of optimization algorithms, and each algorithm has its own advantages [33,34]. Yang X proposed bat algorithm, was introduced for solving engineering optimization tasks [35,36]. The method was based on the echolocation behavior of bats. Cheng MY proposed an algorithm called Symbiotic Organisms Search (SOS) to numerical optimization and engineering design problems [37,38]. SOS simulated the symbiotic interaction strategies adopted by organisms to survive and propagate in the ecosystem. Mirjalili S proposed a novel nature-inspired meta-heuristic optimization algorithm, called Whale Optimization Algorithm (WOA), which mimicked the social behavior of humpback whales [39,40]. In 2017, Mirjalili S proposed an optimization algorithm called Grasshopper Optimization Algorithm (GOA) and applied it to challenge problems in structural optimization [41–43]. Wolpert, D H introduced a new optimization algorithm based on Newton's law of cooling, as called the thermal exchange algorithm (TEO) [44]. The algorithm mainly described that each agent was considered as a cooling object and by associating another agent as environment, a heat transferring and thermal exchange happened between them. Gaurav Dhiman presented a novel bio-inspired algorithm called a seagull optimization algorithm (SOA) for solving computationally expensive problems [45]. The proposed algorithm is able to provide better results as compared to the other well-known metaheuristic algorithms. The algorithm has strong capability in the global search and local optimization.

The improved optimization algorithm is mainly divided into two types: one is to improve the core formula of the optimization algorithm by using the strategy method; the other is to combine the two optimization algorithms. The strategies commonly used by scholars are as follows opposition-based learning [46], Levy-flight [47], Gaussian mutation [48], and so on. Opposition-based learning (OBL) as a new scheme for machine intelligence was introduced by Tizhoosh H R [49]. The foundation of this new approach were estimates and counter-estimates, weights and opposite weights, and actions versus contraction. Trivedi I N used Levy flight improve the Moth-Flame optimization (MFO) [50]. Results showed that applying MFO-LF yielded better facility locations compared other existing algorithms. Chenhua X U proposed an improved gray wolf optimization algorithm applied to solve the function optimization problem. The Gaussian disturbance based the rules of survival of the fittest was given to the global optimum of each generation, thus the algorithm could effectively jump out of local minima [51]. The strategy method can effectively improve part of the ability of the algorithm, while the hybrid algorithm can combine the advantages of two or even more methods, so as to better improve the optimization ability of the algorithm [52,53]. Hybrid optimization algorithms are mainly divided into two types. One is to use a mechanism to select one of the two optimization algorithms for optimization, and use the two algorithms alternately in the iterative process for optimization. The other algorithm used the core formula of one algorithm to improve the other algorithm, and the optimizing ability obtained by different improved positions was also different. Guangqian, D. proposed a hybrid harmony search-simulated annealing method that combines the advantages of each one of the above-mentioned metaheuristic algorithms [54]. The algorithm integrated the position updating formulas of the two optimization algorithms, and selected different position updating formulas for optimization with a certain mechanism, so as to apply to the hybrid wind/photovoltaic/biodiesel/battery system. Alsaeedan proposed hybrid algorithms for WSD that consist of a self-adaptive genetic algorithm (SAGA) and variants of ant colony optimization (ACO) algorithms: max-minant system (MMAS) and ant colony system (ACS) [55]. Aziz M A E examined the ability of two nature inspired algorithms namely: whale optimization algorithm (WOA) and moth-flame optimization (MFO) to determine the optimal multilevel thresholding for image segmentation [56]. The algorithm randomly selected an algorithm for optimization to solve the problem of multi-threshold image segmentation. Karishma Singh proposed a congestion control algorithm based on the multi-objective optimization algorithm named PSOGSA for route optimization and regulating the arrival rate of data from every child node to the parent node [57]. Daniel E proposed an optimum Laplacian wavelet mask (OLWM) based fusion using hybrid cuckoo search-gray wolf optimization (HCS-GWO) for multimodal medical image fusion [58]. This algorithm fully integrated the advantages of the two optimization algorithms, so as to solve the multi-objective problem. Orhan E proposed an effective new hybrid ant colony algorithm based on crossover and mutation mechanism for no-wait flow shop scheduling with the criterion to minimize the maximum completion time [59]. Garg presented a hybrid technique named as a PSO-GA for solving the constrained optimization problems [60]. This algorithm combined the advantages of the two optimization algorithms and proposed a new iterative updating formula. According to the above analysis, hybrid optimization algorithm can better use the advantages of different optimization algorithms to solve the various optimization problem.

In this paper, a 3DPCNN image segmentation algorithm based on HSOA is proposed to solve the complex problem of oil pollution image segmentation. Since the traditional 3DPCNN model has a general effect on oil pollution image segmentation, we use the optimization algorithm to optimize 3DPCNN parameters and improve the segmentation accuracy of the 3DPCNN model, so as to better obtain the oil polluted area in the image. We choose a hybrid optimization algorithm to achieve a balance between exploitation and exploration by taking advantage of SOA and TEO algorithm. In the HSOA algorithm, we improve the TEO algorithm's heat exchange formula to the seagull attack formula in the SOA algorithm, so as to increase the exploitation of the SOA algorithm.

2. Materials and Methods

2.1. Standard 3DPCNN

The PCNN simplified model is a feedback neural network model proposed by simulating the signal processing mechanism of cat visual cortex [61]. In the simplified model, the partial simplification of the parameters makes the generality of the model well guaranteed. However, there is a great difference in the response of the visual system to the different feature regions in the image. In the PCNN model, this difference is mainly reflected in the setting of the parameters, and the flexible changes in the parameters still affect the final fusion results [62]. Therefore, this paper uses the most commonly discrete mathematical iterative models. The simplified model is shown in Figure 1.
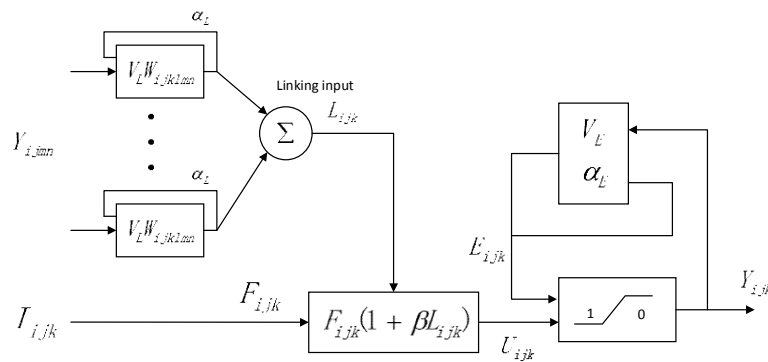

Figure 1. Model of 3DPCNN neuron.

The mathematical expression of the PCNN simplified model can be expressed by

$$F_{ijk}(n) = I_{ijk} \tag{1}$$

$$L_{ijk}(n) = \exp(-\alpha_L)L_{ij}(n-1) + V_L \sum W_{ijklmn} Y_{ijmn}(n-1) \tag{2}$$

$$U_{ijk}(n) = F_{ijk}(1 + \beta L_{ijk}(n)) \tag{3}$$

$$Y_{ijk}(n) = \begin{cases} 1, & U_{ijk}(n) > \theta_{ijk}(n-1) \\ 0, & U_{ijk}(n) \leq \theta_{ijk}(n-1) \end{cases} \tag{4}$$

$$E_{ijk}(n) = e^{-\alpha_E}E_{ijk}(n-1) + V_E Y_{ij}(n) \tag{5}$$

where n is the number of iterations; I_{ijk} is the external input; $Y_{ijk}(n)$ is the output of neuron; U_{ijk} is the internal behavior of neurons; $F_{ijk}(n)$ is feedback, input excitation; $L_{ijk}(n)$ is the input of neuron's link; W_{ijklmn} is the weight coefficient of the connection between neurons; β is the link strength coefficient; θ_{ijk} is the output of variable threshold function; V_L and α_L are, respectively, the signal amplification factor and attenuation time constant of neuron's link; V_E and α_E are, respectively, the signal amplification factor and decay time constant of variable threshold function.

2.2. 3D Linked Weight W

Weights W_{ijklmn} are used to connect the neighbouring neurons in the feeding and linking channels, which are responsible for transmitting some information from neighbours. In order to reflect the information of color images, 26 neighborhood linked matrices are adopted to expand the information in the 3D space acceptable to neurons, which can make better use of the information in color images and improve the precision of segmentation. As shown in Figure 2, it shows the 26 neighborhood linked matrices. The intermediate neurons can transmit information to 26 neurons in 3D through the ignition. The figure is divided into three channels, which correspond to the feedback output of the three color components of R, G, and B in the color image. The linked matrix is convolved with the color image.

The fluctuation caused by ignition of each pixel can cause the fluctuation of other pixel points, and the ignition information of each pixel in the color space can be observed. Thus, information utilization in the color image can be realized and image segmentation can be realized.
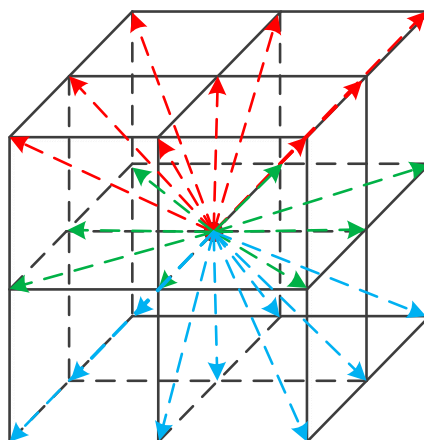

Figure 2. 26 neighborhood linked matrix.

In the segmentation of color images by 3DPCNN, the color images are viewed as the data matrix. The data matrix is convolved by the linked matrix, and binary pulse sequences Y generated through the pulse generation region. The 3D integral segmentation method processes the whole information of the color image, breaks the spatial information limitation of the 2D segmentation method and reduces the computational complexity.

2.3. Fitness Function

In order to solve the problem of high parameter complexity, long operation time and low segmentation precision of the 3D-PCNN image segmentation algorithm, HSOA optimizes the searching process of model parameters. For better solutions, the selection of fitness functions is very important. In this paper, application and product cross entropy as the fitness function of HSOA, by calculating the minimum cross entropy to search the parameter optimal solution. The minimum cross entropy is to represent the differences between the different probability distributions using the cross entropy represented by the following convex function, and there is always a threshold to reduce the amount of information on the front and back of the image, and the minimum cross entropy can be used to evaluate the image segmentation result by calculating the entropy of this threshold [39,40]. Cross entropy describes information differences between probability distributions $P = \{P_1, P_2, \cdots, P_N\}$ and $Q = \{Q_1, Q_2, \cdots, Q_N\}$. It can be expressed by

$$D(P : Q) = \sum_{i=1}^{N} p_i \times \ln \frac{p_i}{q_i} + \sum_{i=1}^{N} q_i \times \ln \frac{q_i}{p_i} \tag{6}$$

In image segmentation, P is the original image and Q is the segmented image. Equation (6) is taken as the fitness function of HSOA, and the parameters E and β_1 of the 3D-PCNN model are optimized at the same time. When D is the minimum, the optimal solution obtained is input into the 3D-PCNN model, and the segmentation result graph is output.

2.4. Seagull Optimization Algorithm

Seagulls, scientific named as Laridae, are sea birds which can be found all over the planet. There is a wide range of seagull species with different masses and lengths. Seagulls are omnivorous and eat insects, fish, reptiles, amphibians, earthworms, and so on. Body of most seagulls is covered with white plumage. Seagulls are very intelligent birds. They use bread crumbs to attract fish and produce

rain-like sound with their feet to attract earthworms hidden under the ground. Seagulls can drink both fresh and salt water [45], that can be seen in Figure 3.
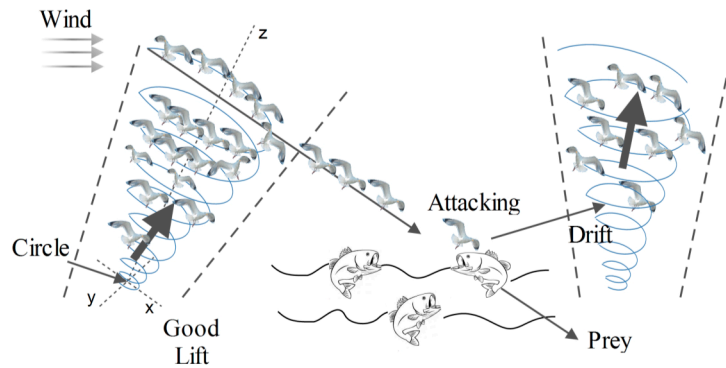

Figure 3. Migration and attacking behaviors of seagulls.

The mathematical models of migration and attacking the prey are discussed. During migration, the algorithm simulates how the group of seagulls moves towards one position to another. A seagull should satisfy the conditions:

To avoid the collision between neighbors, an additional variable A is employed for the calculation of new search agent position.

$$C_s = A \cdot P_s \tag{7}$$

where C_s represents the position of search agent which does not collide with other search agent, P_s represents the current position of search agent, x indicates the current iteration, and A represents the movement behavior of search agent in a given search space.

$$A = f_c - (x \cdot (f_c / Max_{iteration})) \tag{8}$$

where f_c is introduced to control the frequency of employing variable A which is linearly decreased from f_c to 0.

After avoiding the collision between neighburs, the search agents are move towards the direction of best neighbor.

$$M_s = B \cdot (P_{bs}(x) - P_s(x)) \tag{9}$$

where, M_s represents the positions of search agent P_S towards the best fit search agent P_{bs}. The behavior of B is randomized, which is responsible for balancing between exploration and exploitation properly. B is calculated as:

$$B = 2 \cdot A^2 \cdot rd \tag{10}$$

where, rd is a random number lies in the range of [0,1].

Lastly, the search agent can update its position with respect to best search agent by:

$$D_S = |C_S + M_S| \tag{11}$$

where, D_S represents the distance between the search agent and best fit search agent.

The exploitation intends to exploit the history and experience of the search process. While attacking the prey, the spiral movement behavior occurs in the air. This behavior in x, y, and z planes is described as follows.

$$x' = r \cdot \cos(k) \tag{12}$$

$$y' = r \cdot \sin(k) \tag{13}$$

$$z' = r \cdot k \tag{14}$$

$$r = u \cdot e^{kv} \tag{15}$$

where r is the radius of each turn of the spiral, k is a random number in range $[0 \leq k \leq 2\pi]$. u and v are constants to define the spiral shape, and e is the base of the natural logarithm. The updated position of search agent is calculated using (13)–(16).

$$P_s(x) = (D_s \cdot x' \cdot y' \cdot z') + P_{bs}(x) \tag{16}$$

where, P_s saves the best solution and updates the position of other search agents.

2.5. Thermal Exchange Optimization

The TEO is a new optimization algorithm based on Newton's law of cooling, which the rate of heat loss of a body is proportional to the difference in temperatures between the body and its surroundings [44]. Transferring heat to the surrounding environment of hot iron objects is shown in Figure 4.

Figure 4. Hot iron objects, transferring heat to the surrounding environment.

In TEO algorithm, some agents are defined as the cooling objects and the remaining agents are supposed to represent the environment. Updating the temperature formula between objects can be defined as:

$$T_i^{env} = (1 - (c_1 + c_2 \cdot (1 - t)) \cdot random) \cdot T_i'^{env} \tag{17}$$

$$t = \frac{l}{L} \tag{18}$$

where c_1, c_2 are the controlling variables, $T_i'^{env}$ is the previous temperature of the object, which is modified to T_i^{env}. l is the current iteration number, L is the max iteration number.

According to the previous steps and Equation (19), new temperature of each object is updated by

$$T_i^{new} = T_i^{env} + (T_i^{old} - T_i^{env}) \exp(-\beta t) \tag{19}$$

$$\beta = \frac{\text{Cost}(object)}{\text{Cost}(worst \quad object)} \tag{20}$$

where, the nature when an object has lower β, it exchanges the temperature slightly. The value of β for each object is evaluated according Equation (20).

To prevent the temperature of object from falling into local optimum, we can adjust the parameter Pro. It is specified whether a component of each cooling object must be changed or not. If rand < Pro, one dimension of the i th agent is selected randomly and its value is regenerated as follows:

$$T_{i,j} = T_{i,\min} + rand \cdot (T_{j,\max} - T_{j,\min}) \tag{21}$$

where, $T_{i,j}$ is the j th variable of the ith agent. $T_{j,\max}$ and $T_{j,\min}$ are the lower and upper bounds of the j th variable.

3. Proposed Method

3.1. Hybrid Seagull Optimization Algorithm (HSOA)

In this subsection, the Hybrid SOA describes in detail. The SOA algorithm simulates the mathematical model established by the feeding habits of seagulls, and the mathematical formula such as Equation (9) when prey attacks. It can be seen from the formula that B is responsible for balancing between exploration and exploitation properly, as shown in Equation (10), and its moving speed is slow, which makes the aggressiveness of seagulls not strong and the ability to seek for the best work. In order to solve this problem, we apply the idea of thermal exchange in TEO algorithm to enhance the local optimization ability of seagulls. In the Equation (19), β exchanges the temperature slightly between objects so as to get close to the target object quickly. In this paper, β is improved Equation (9) so that seagulls can better move towards prey. Its mathematical formula is as follows:

$$M_s = B \cdot (P_{bs}(x) - P_s(x)) \cdot \exp(-\beta t) \tag{22}$$

3.2. Proposed Multi-Segmentation Method

In resolution of color image segmentation, that parameters in the 3D-PCNN model need to rely on the prior knowledge, determination, the exponential decay results in increased operation time and slow partition calculation, and the 3D-PCNN model based on HSOA is proposed in this paper. The exponential decay value function in the model is reduced to the threshold function E and β as compared to the 3D-PCNN model. It uses that HSOA to find the optimal solution of the threshold value E and the connecting intensity constant. It can be seen from Figure 5.
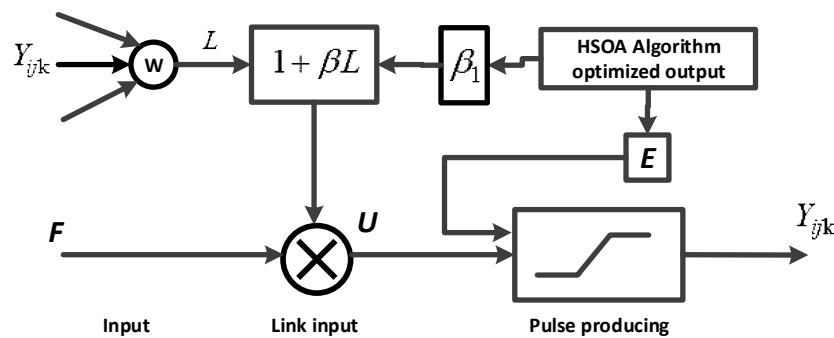

Figure 5. 3DPCNN-HSOA model.

The mathematical expression of the 3DPCNN-HSOA simplified model can be expressed by

$$
\begin{cases}
F_{ijk}(n) = I_{ijk} \\
L_{ijk}(n) = \exp(-\alpha_L)L_{ij}(n-1) + V_L\sum W_{ijklmn}Y_{ijmn}(n-1) \\
U_{ijk}(n) = F_{ijk}(1 + \beta_1 L_{ijk}(n)) \\
Y_{ijk} = \begin{cases} 1 & U_{ijk}(n) > E \\ 0 \end{cases} \\
P_s^{Levy} = (D_s \cdot x' \cdot y' \cdot z') + P_{bs}(x) \\
M_s = B \cdot (P_{bs}(x) - P_s(x))\exp(-\beta t)
\end{cases}
\tag{23}
$$

where, P_x^{Levy} is the location of individual particles that the HSOA needs to optimize, E and β_1 are two independent particles in the proposed optimization algorithm. The optimal fitness function F_j is optimized by the HSOA. And then, the optimization algorithm finds the best particles E and β_1, and input particles into the model to get a binary color image. The flowchart of the HSOA can be seen from Figure 6.
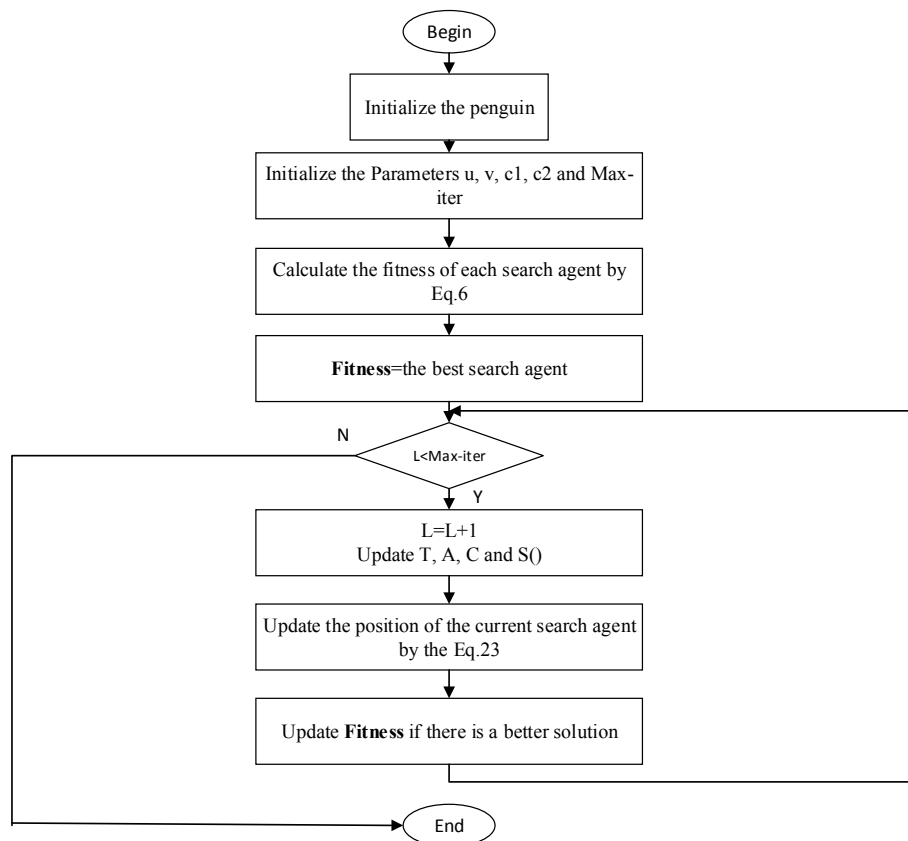

Figure 6. The flowchart of the HSOA.

The computational complexity of the proposed method 3DPCNN-HSOA depends on the number of each combination (L), the number of generations (g), the number of population (n) and the parameter dimensions (d). So, 3DPCNN's computational complexity of L combination is $O(L)$. The computational complexity of the seagull population location update is $O(n \times d)$. The calculation of fitness function values of all seagull populations is $O(n \times L)$. Therefore, the final computational complexity of the proposed method is:

$$
O(3DPCNN, HSOA) \approx O(g \times (n \times d + n \times L))
\tag{24}
$$

4. Satellite Images Experiments and Results

In this chapter, HSOA algorithm is applied to optimize the MCE function of 3DPCNN algorithm. In order to better verify the image segmentation ability of 3DPCNN-HSOA algorithm, it is compared with the optimized 3DPCNN algorithm of WOA, PSO, FPA and BA. The color image has three color channels. In this paper, the images of the three channels are segmented, and then the three resulting images are fused to obtain the final segmentation result graph. Firstly, the segmentation effect and precision of 3DPCNN-HSOA algorithm are analyzed. Then the segmentation ability, statistical analysis and stability analysis of the proposed HSOA algorithm and other optimization algorithms in 3DPCNN image segmentation are analyzed. Finally, the Berkeley image library is tested and analyzed. All parameters of the comparison optimization algorithm are shown in Table 1.

Table 1. Parameters and references of the comparison algorithms.

Algorithm	Parameters	Value
SOA	u	1
	v	0.001
	a	[0.2]
WOA [63]	b	1
	l	[−1,1]
FPA [64]	P	0.5
	Swam size	200
PSO [65]	Cognitive, social acceleration	2,2
	Inertial weight	0.95–0.4
BA [66]	β	(0,1)

The test images [67] in this paper are as follows Figure 7. Color image segmentation requires a higher threshold level, so it is more complex to use optimization technology to solve the problem. Therefore, the optimization algorithm has the characteristics of randomness. So, all image segmentation experiments are run separately for 30 times. The parameters for the 3D-PCNN model are given as follows. In the 3D-PCNN model, $F_{ijk} = 0.1$, $\alpha_L = 0.7$, $V_L = 1.0$, $V_T = 2000$. V_T must be large enough to ensure that every neuron of the 3D-PCNN is permitted to fire only once. The above parameters are manually set by experiments.
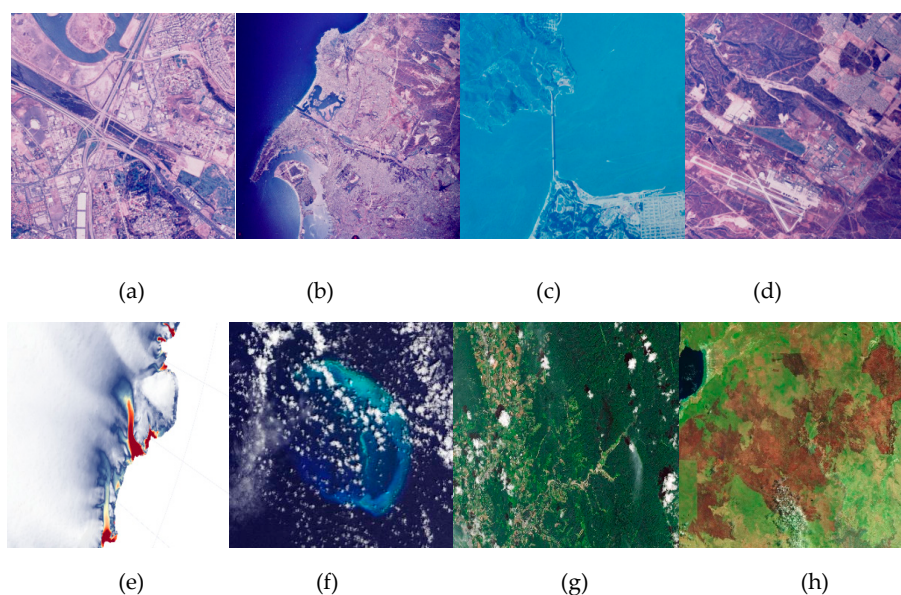

(a)   (b)   (c)   (d)

(e)   (f)   (g)   (h)

Figure 7. The color test images. (**a**) Satellite image1; (**b**) Satellite image2; (**c**) Satellite image3; (**d**) Satellite image4; (**e**) Satellite image5; (**f**) Satellite image6; (**g**) Satellite image7; and (**h**) Satellite image8.

4.1. Comparison with WOA, FPA, PSO, and BA Algorithm based 3DPCNN

In this experiment, to show the merits of proposed 3DPCNN-HSOA technique, the results are compared with WOA, FPA, PSO, and BA use same objective function (3DPCNN). The evaluation indexes of segmentation result images include Peak Signal-to-Noise Ratio (PSNR) [68] and feature similarity (FSIM) [69]. From Table 2, it can be observed that the result of the PSNR and FSIM for all the test images, HSOA is better and more reliable than WOA, FPA, PSO, and BA, because of its precise search capability. Performance of WOA and BA has closely followed HSOA. The solution update strategy for FPA and PSO may have led to poor results. The good results based on the HSOA algorithm are shown in Table 2, and the 3DPCNN-HSOA algorithm performs best in color images such as satellite images.

Table 2. The PSNR and FSIM of each algorithm under 3DPCNN.

T	WOA		FPA		PSO		BA		HSOA	
	PSNR	FSIM	PSNR	FSIM	PSNR	FSIM	PSNR	FSIM	PSNR	FSIM
Satellite image1	17.9744	0.8654	17.5541	0.7738	16.9008	0.7734	17.8235	0.8679	23.3737	0.94884
Satellite image2	22.3392	0.8277	22.3470	0.8280	22.3044	0.8380	19.9078	0.7768	26.2123	0.93556
Satellite image3	20.9181	0.7749	20.9579	0.7750	20.5956	0.6997	20.9783	0.7750	26.4849	0.93772
Satellite image4	18.9191	0.7835	18.3870	0.7677	19.1694	0.7289	15.6841	0.6772	26.2893	0.9152
Satellite image5	18.1830	0.7560	18.1572	0.7571	17.3974	0.3912	18.2168	0.7569	21.1809	0.91668
Satellite image6	22.4419	0.8542	21.1909	0.8160	21.0133	0.7716	22.5738	0.8542	22.9081	0.85038
Satellite image7	17.2417	0.7913	16.8802	0.8247	16.9702	0.7810	16.8993	0.7749	23.4707	0.92476
Satellite image8	17.1414	0.7444	16.4690	0.7612	17.8660	0.8831	17.2795	0.8600	27.0487	0.89289

For visual qualitative analysis, the performance of this method is shown in Figures 8–15. The performance of the FPA is the worst, can be seen from the Figure 10b, Figure 12b, and Figure 14b. Figures 14c and 15c have the under-segmentation, so the PSO algorithm has a bad visual qualitative. It can be seen from Figures 8 and 9 that the performance of the WOA and BA have a good visual qualitative. The HSOA algorithm can achieve a satisfactory segmentation effect with good edge preservation from all test images. Therefore, the visual results show that 3DPCNN-HSOA achieves a good segmentation effect by accurately identifying the complex target and background in satellite image segmentation.
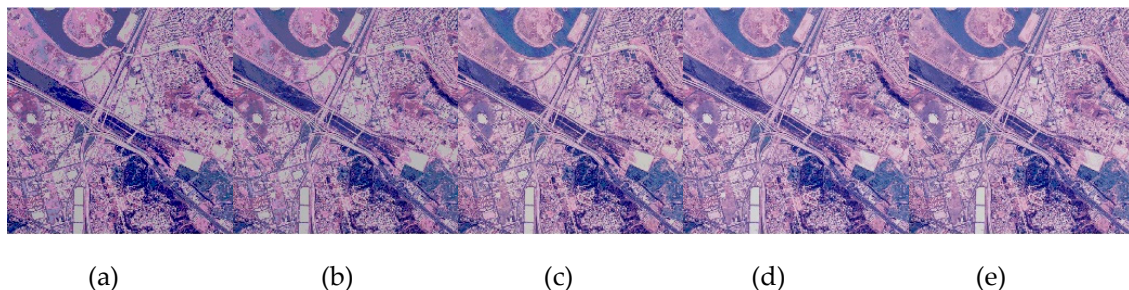

(a)   (b)   (c)   (d)   (e)

Figure 8. The segmented results of Satellite image1. (**a**) WOA; (**b**) FPA; (**c**) PSO; (**d**) BA; and (**e**) HSOA.

(a)　　　　　(b)　　　　　(c)　　　　　(d)　　　　　(e)
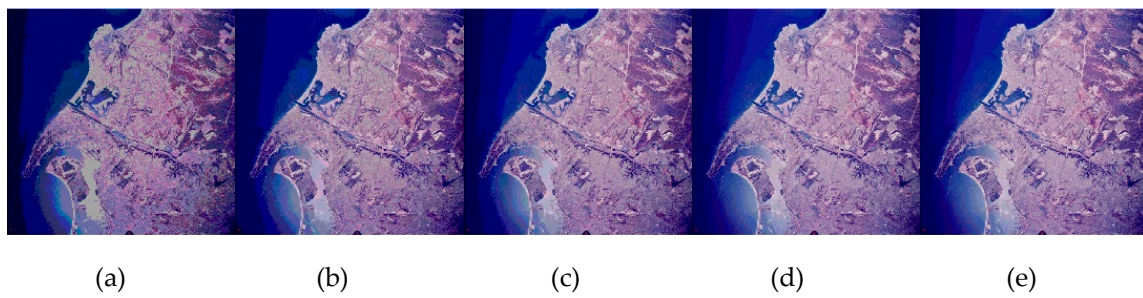
Figure 9. The segmented results of Satellite image2. (**a**) WOA; (**b**) FPA; (**c**) PSO; (**d**) BA; and (**e**) HSOA.

(a)　　　　　(b)　　　　　(c)　　　　　(d)　　　　　(e)
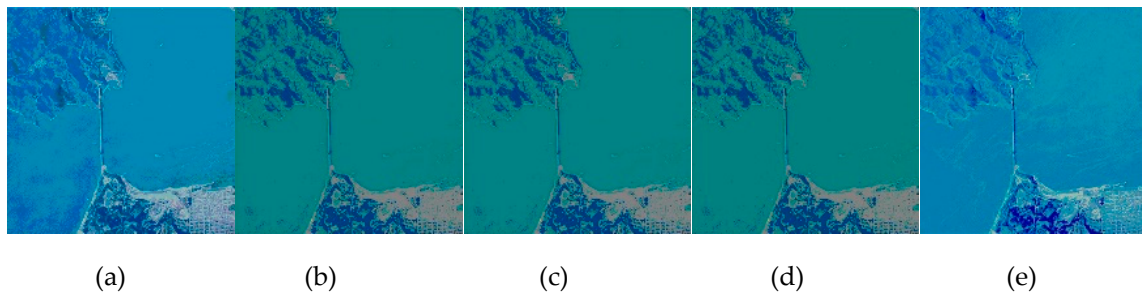
Figure 10. The segmented results of Satellite image3. (**a**) WOA; (**b**) FPA; (**c**) PSO; (**d**) BA; and (**e**) HSOA.

(a)　　　　　(b)　　　　　(c)　　　　　(d)　　　　　(e)
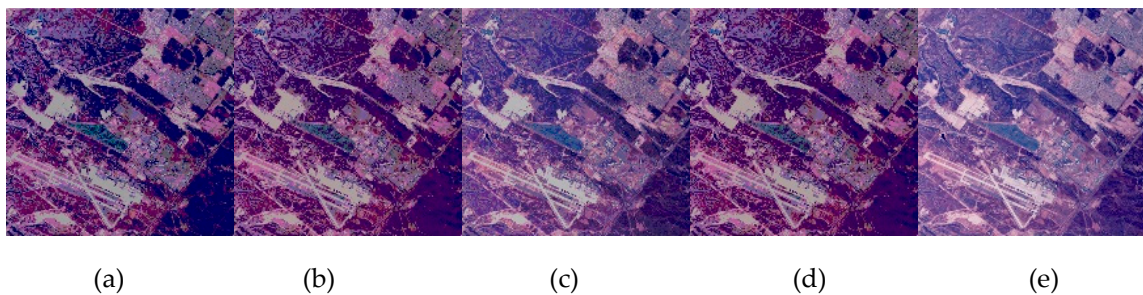
Figure 11. The segmented results of Satellite image4. (**a**) WOA; (**b**) FPA; (**c**) PSO; (**d**) BA; and (**e**) HSOA.

(a)　　　　　(b)　　　　　(c)　　　　　(d)　　　　　(e)
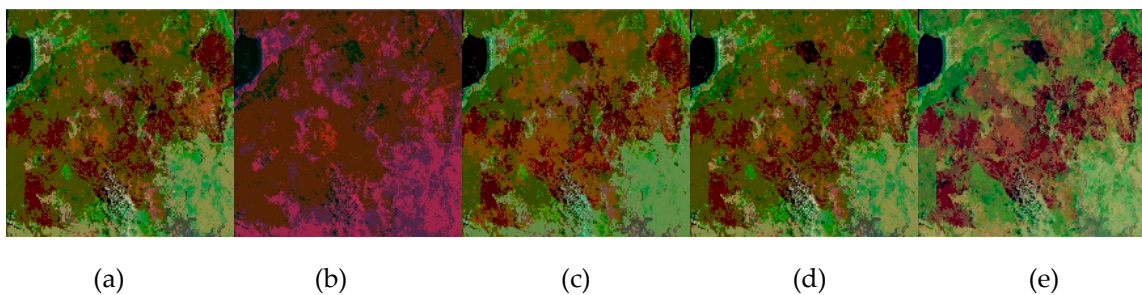
Figure 12. The segmented results of Satellite image5. (**a**) WOA; (**b**) FPA; (**c**) PSO; (**d**) BA; and (**e**) HSOA.

(a)　　　　　(b)　　　　　(c)　　　　　(d)　　　　　(e)
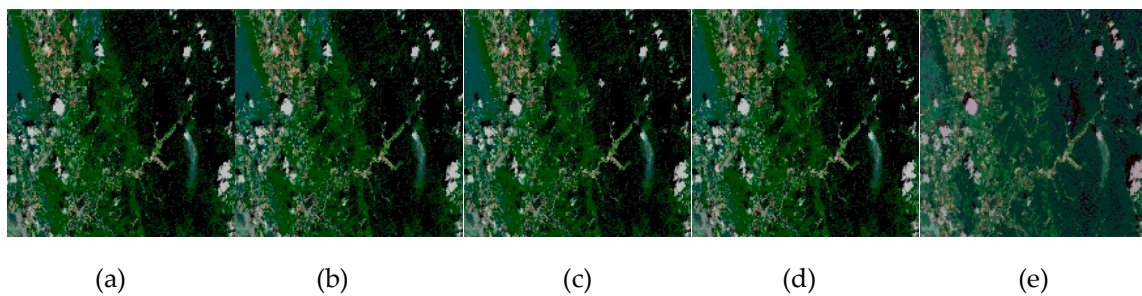
Figure 13. The segmented results of Satellite image6. (**a**) WOA; (**b**) FPA; (**c**) PSO; (**d**) BA; and (**e**) HSOA.
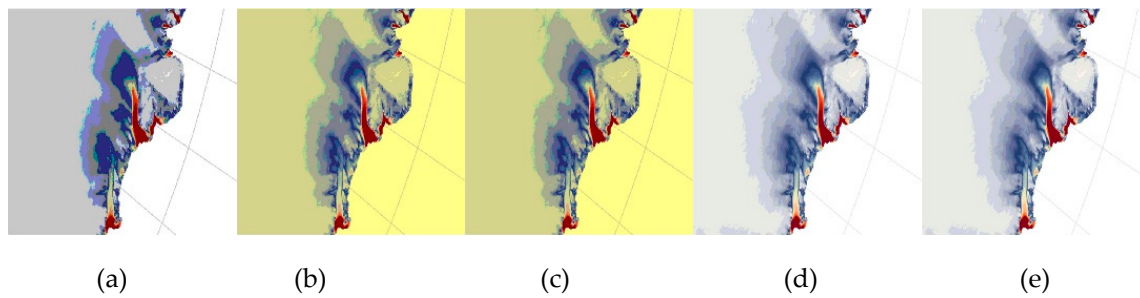
Figure 14. The segmented results of Satellite image7. (**a**) WOA; (**b**) FPA; (**c**) PSO; (**d**) BA; and (**e**) HSOA.
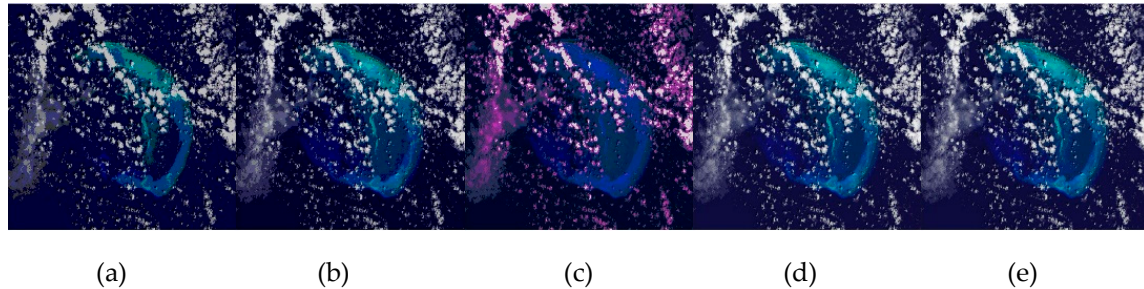
Figure 15. The segmented result of Satellite image8. (**a**) WOA; (**b**) FPA; (**c**) PSO; (**d**) BA; and (**e**) HSOA.

4.2. Stability and Statistical Analysis

Based on the natural optimization algorithm, the results of each run are not the same. Therefore, in order to analyze the stability of the proposed algorithm based on 3DPCNN-HSOA, we use the value of standard deviation (STD). The STD can be intuitive to the operational stability of the algorithm, and the lower the value of the algorithm, the stronger the robustness of the algorithm. Table 3 shows the STD values of each algorithm after 30 runs. It can be seen from the table that the stability of HSOA algorithm is the strongest, especially when dealing with the segmentation of satellite images, its stability is obviously better than other comparison algorithms, indicating that 3DPCNN-HSOA algorithm has a good segmentation ability, and can find the optimal threshold of the image better, more accurate, and more stable.

Table 3. Comparison of standard deviation (STD) of FSIM computed by WOA, FPA, PSO, BA, and HSOA using 3DPCNN as an objective function.

Test Images	WOA	FPA	PSO	BA	HSOA
Satellite image1	9.6048E-08	1.0350E-07	5.4459E-08	2.3562E-08	9.4807E-16
Satellite image2	9.2569E-08	9.3650E-08	1.0614E-07	6.3755E-08	4.0982E-15
Satellite image3	3.9561E-08	3.9770E-08	2.6169E-08	7.3730E-08	3.5838E-10
Satellite image4	2.6712E-08	6.4477E-08	5.5728E-02	1.8992E-08	4.5094E-12
Satellite image5	1.0176E-07	6.1097E-08	2.0845E-08	8.6422E-08	2.2787E-15
Satellite image6	5.0916E-08	6.2483E-08	1.0282E-07	1.0859E-07	3.4058E-12
Satellite image7	1.0878E-07	1.0263E-07	1.8820E-05	2.9401E-08	2.1315E-11
Satellite image8	7.4459E-08	6.4278E-08	4.4221E-08	6.6786E-09	4.5382E-16

We statistically analyze the experimental results to better observe the differences between algorithms. We use Wilcoxon rank sum test [70], a nonparametric statistical test that checks whether one of two independent samples is larger than the other. We calculate the p-value of FSIM of HSOA algorithm and WOA, FPA, PSO, and BA algorithm. The experimental statistical results are shown in Table 4. If the p-value of the two algorithms is greater than 0.05, there is no significant difference between the two algorithms. On the other hand, a p-value less than 0.05 means that there is a significant difference between the two algorithms at the significance level of 5%. It can be seen from Table 4 that 3DPCNN-HSOA algorithm is obviously better than the comparison algorithm in the statistical sense.

Table 4. The calculated p-values from the Wilcoxon test for the 3DPCNN-HSOA versus other optimizers.

Test Images	WOA	FPA	PSO	BA
Satellite image1	P < 0.05	P < 0.05	P < 0.05	P < 0.05
Satellite image2	P < 0.05	P < 0.05	P < 0.05	P < 0.05
Satellite image3	P < 0.05	P < 0.05	P < 0.05	P < 0.05
Satellite image4	P < 0.05	P < 0.05	P < 0.05	P < 0.05
Satellite image5	P < 0.05	P < 0.05	P < 0.05	P < 0.05
Satellite image6	P < 0.05	P < 0.05	P < 0.05	P < 0.05
Satellite image7	P < 0.05	P < 0.05	P < 0.05	P < 0.05
Satellite image8	P < 0.05	P < 0.05	P < 0.05	P < 0.05

4.3. Compared with the Latest Satellite Image Method

In order to better test the segmentation capability of the 3DPCNN-HSOA model for satellite images, we compare it with the new segmentation method for satellite images, such as Fully Convolutional Networks (FCN) [71], An Image-Segmentation-Based Framework (ISBF) [72], and SOM-PCNN [73]. We experimented with eight satellite images. The PSNR value, FSIM value, and CPU time of the segmentation result are calculated, as shown in Table 5. The table records the mean and variance values of eight satellite images.

Table 5. The result of the compared satellite image segmentation method.

T	PSNR		FSIM		CPU TIME	
	MEAN	STD.	MEAN	STD.	MEAN	STD.
FCN	22.3470	7.39E-08	0.8980	6.97E-03	13.2145	3.21E-05
ISBF	22.3392	7.40E-08	0.8880	5.14E-08	4.2146	4.21E-04
SOM-PCNN	23.9181	6.97E-03	0.9080	3.21E-05	15.2142	**5.21E-07**
3DPCNN-HSOA	**24.6211**	**5.21E-09**	**0.9153**	**4.84E-11**	**2.0145**	6.65E-06

As can be seen from Table 5, the results of 3DPCNN-HSOA model are better than other comparison algorithms. The results of SOM-PCNN and FCN perform better, but their operation time is longer. Although the ISBF algorithm has low accuracy, its running time is better than SOM-PCNN and FCN. The 3DPCNN-HSOA model not only ensures the accuracy, but also reduces the computation time, which indicates that the HSOA algorithm has a strong optimization ability and finds the best parameters of the 3DPCNN-HSOA model quickly and accurately, and finally obtains the best segmentation result of the image.

5. Oil Pollution Images Experiments and Results

In this experiment, for further showing the merits of 3DPCNN-HSOA method, the comparison is performed with other classical image segmentation algorithms, such as A Level Set Approach (LSA) [74], multilevel thresholding (MS) [75] and the optimal Color Image Multilevel Thresholding Technique (GLCM) [76]. The images of the experiment are taken by a drone in the field, such as the Figure 16. As can be seen from Figure 16, (a) and (b) show that the oil pollution area is relatively obvious, while the oil pollution area of (c) and (d) has large interference, which brings great difficulties to the segmentation algorithm and can better verify the segmentation ability of the algorithm. This section uses an extensive comparative study on oil pollution by using performance metrics like Probability Rand Index (PRI), Variation of Information (VoI), Global Consistency Error (GCE), and Boundary Displacement Error (BDE) [77,78]. Table 6 shows the average results of PRI, BDE, GCE, and VoI of the oil pollution images.
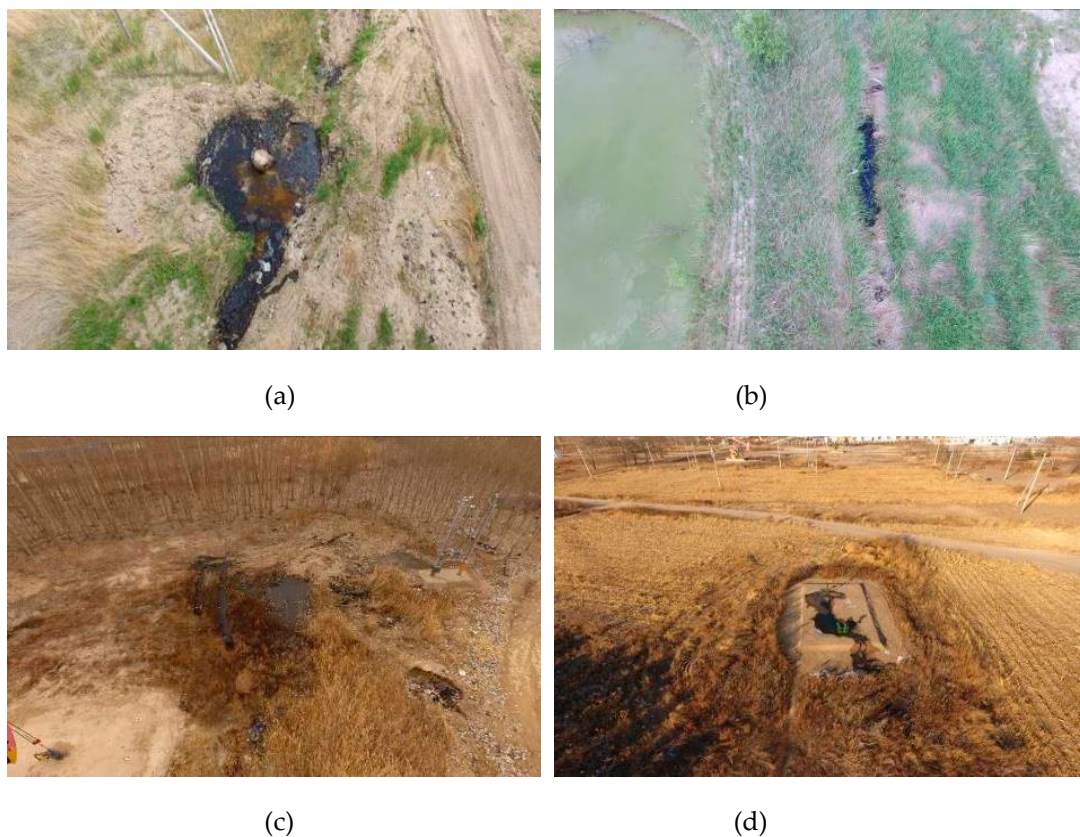
(a)

(b)

(c)

(d)

Figure 16. The segmentation results of oil pollution images. (**a**) oil pollution1; (**b**) oil pollution2; (**c**) oil pollution3; and (**d**) oil pollution4.

Table 6. The comparison results for the 3DPCNN-HSOA versus other optimizers.

ALGORITHM	BDE	PRI	GCE	VOI	TIME
3DPCNN-HSOA	**8.3161**	**0.7774**	**0.2586**	**3.2826**	**1.8415**
LSA	10.2151	0.7255	0.2954	3.6661	5.2141
MS	8.9881	0.7125	0.2865	3.5841	3.5147
GLCM	8.8541	0.7188	0.3011	3.8414	10.3214

Figures 17–20 shows the image segmentation results of each algorithm. Since there is no clear index for the oil pollution area actually photographed, we use Photoshop (PS) to segment the oil pollution area in the original image and take the segmentation result as the ground truth for comparison, and the subsequent indexes will be calculated according to the ground truth figure. As can be seen from the figure, 3DPCNN-HSOA can effectively segment the oil pollution area from the complex background. The LSA algorithm has a better effect on the oil pollution image with a simple background, as shown in Figures 17b and 18b, but Figure 17b has an over-segmentation phenomenon, and the redundant area is divided. When the LSA algorithm is used to segment complex images, the oil pollution area cannot be obtained and the segmentation effect is the worst, as shown in Figures 19b and 20b. The segmentation results of MS and GLCM algorithm are similar, but it can be seen from Figures 19 and 20 that the segmentation results of GLCM are better than that of MS, and the oil pollution area is more obvious. At the same time, the oil pollution boundary of MS is relatively fuzzy.
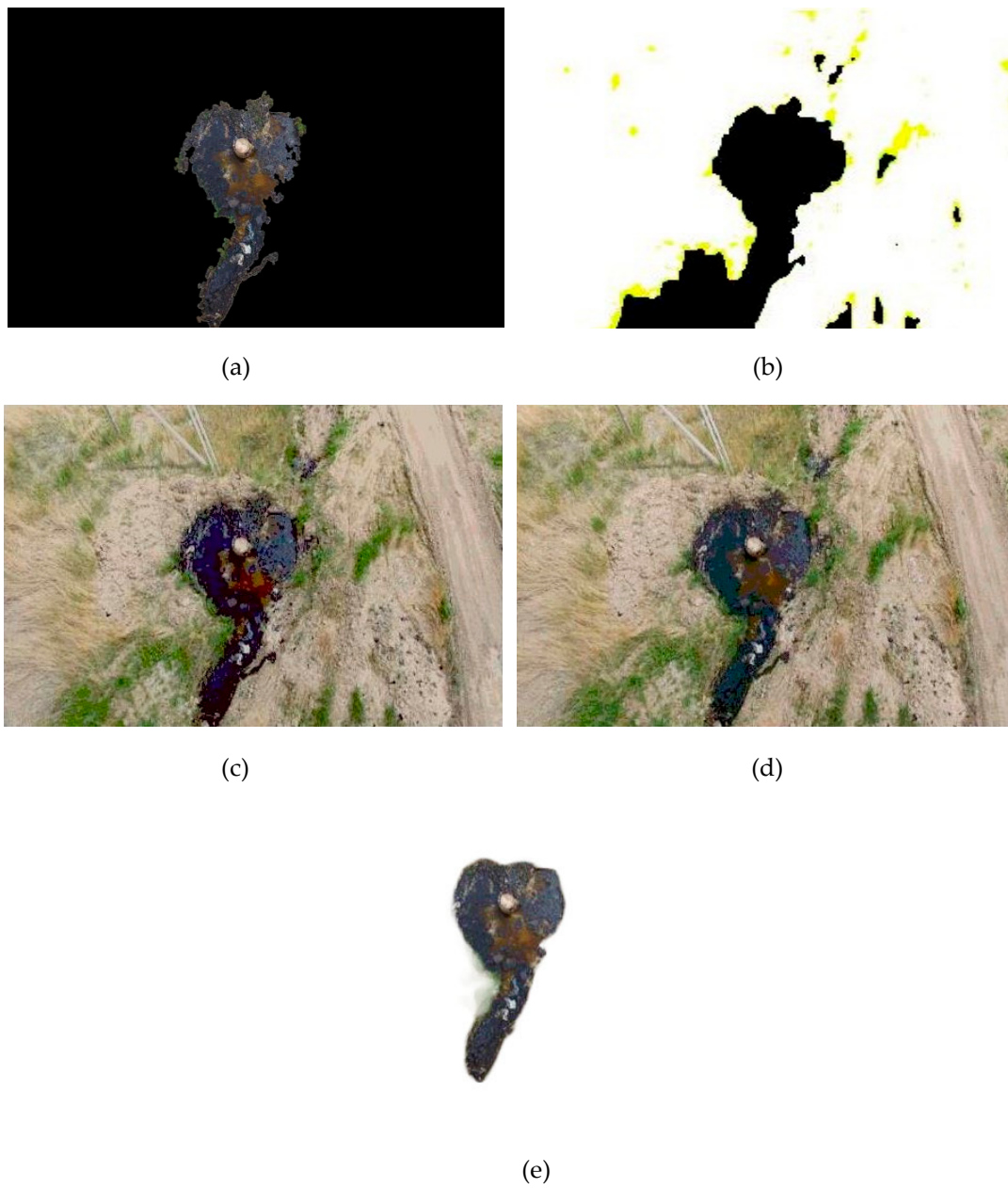
(a)

(b)

(c)

(d)

(e)

Figure 17. The segmentation results of oil pollution1 image. (**a**) 3DPCNN-HSOA; (**b**) LSA; (**c**) MS; (**d**) GLCM; and (**e**) Ground truth.

(a)

(b)

Figure 18. *Cont.*

(c)

(d)

(e)
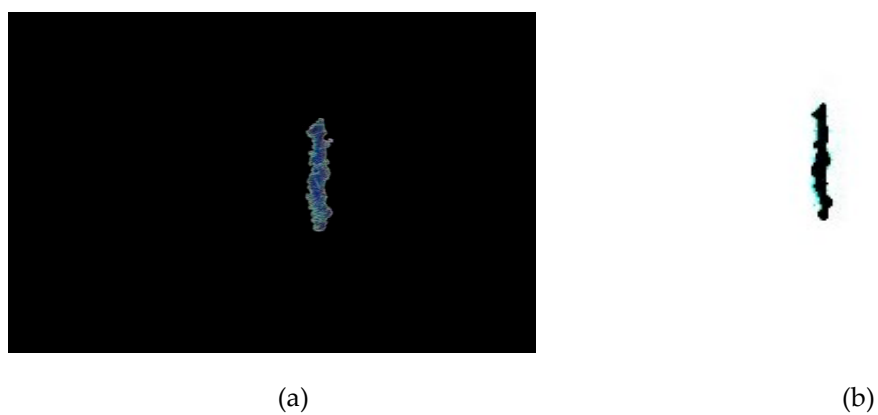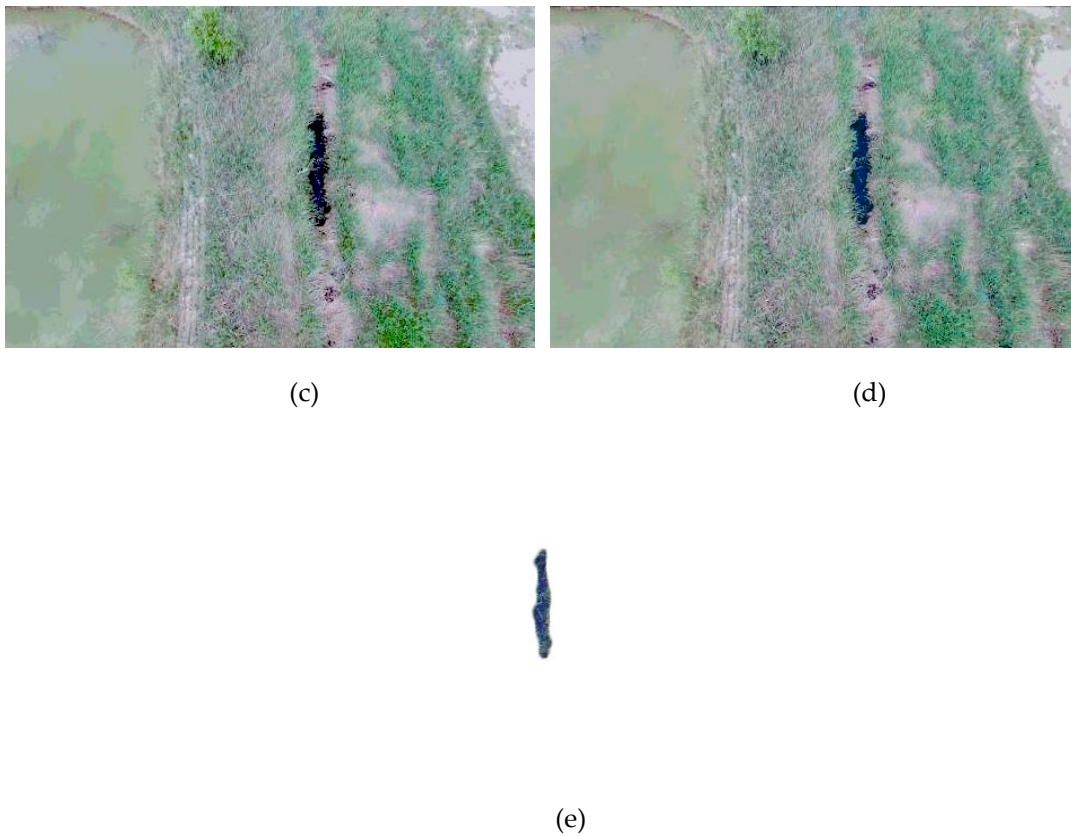
Figure 18. The segmentation results of oil pollution2 image. (**a**) 3DPCNN-HSOA; (**b**) LSA; (**c**) MS; (**d**) GLCM; and (**e**) Ground truth.

(a)

(b)

(c)

(d)

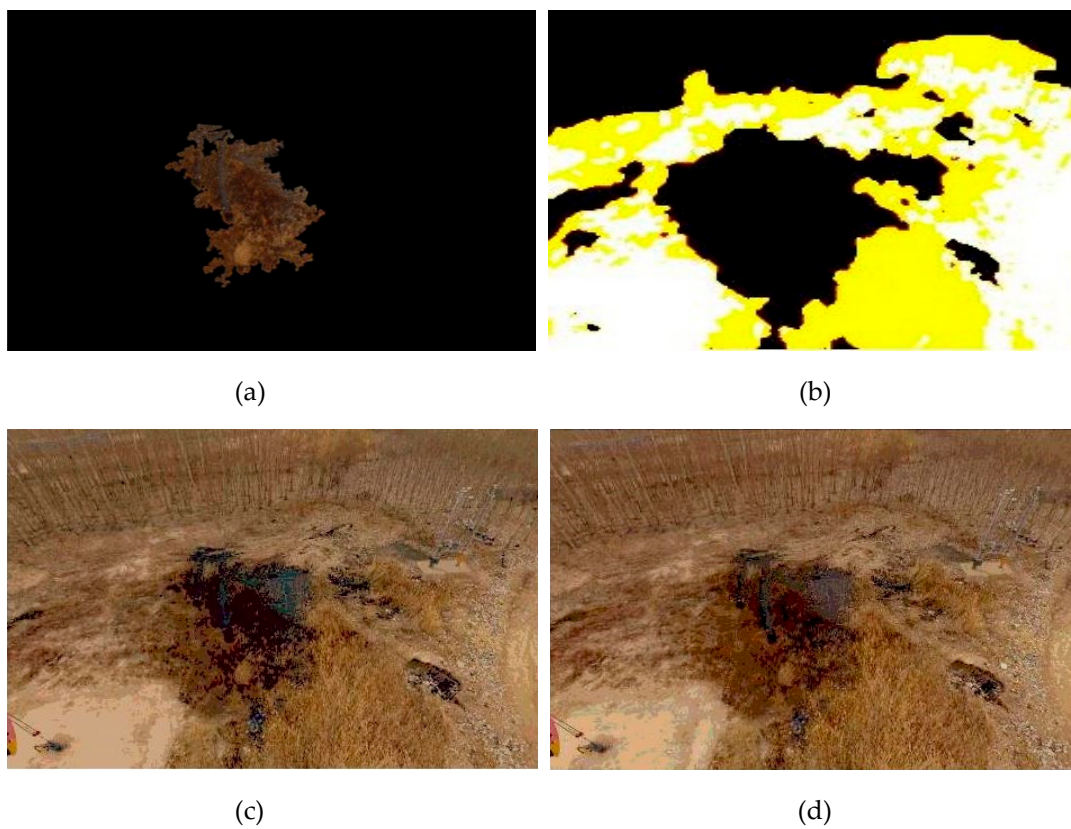**Figure 19.** *Cont.*

(e)

Figure 19. The segmentation results of oil pollution3 image. (**a**) 3DPCNN-HSOA; (**b**) LSA; (**c**) MS; (**d**) GLCM; and (**e**) Ground truth.

(a)

(b)

(c)

(d)

(e)

Figure 20. The segmentation results of oil pollution4 image. (**a**) 3DPCNN-HSOA; (**b**) LSA; (**c**) MS; (**d**) GLCM; and (**e**) Ground truth.

From the visual analysis and data results of the image segmentation results of oil pollution, it can be seen that the 3DPCNN-HSOA algorithm has a good ability for the image segmentation of oil pollution, and its time is relatively short.

The results displayed in Table 6, that the proposed technique outperforms all other compared image segmentation algorithms. It can be seen from the table that the numerical value of 3DPCNN-HSOA algorithm is the best, indicating that the segmentation effect is the best. And the MS model segmentation effect is the most check. LSA and GLCM segmentation effect is not much different. The CPU running time of 3DPCNN-HSOA algorithm is the shortest, followed by GLCM and MS, and the running time of LSA algorithm is the slowest. According to the comparison between the results of image segmentation algorithms, the segmentation accuracy of 3DPCNN-HSOA algorithm is higher and its stability is better than other comparison algorithms. Therefore, the algorithm proposed in this paper has strong robustness, can complete the complex image segmentation task in a relatively short CPU time, and obtain good segmentation results with excellent segmentation accuracy.

6. Discussion

Oil pollution brings great damage to the environment. Oil leakage includes Oil spill and oil and gas drilling. The offshore oil spill has a large area of pollution and a long time of damage, and some damages are irreversible. Oil and gas drilling is widespread, oil is used in major equipment, the area of its contaminated continent is not easy to find, and the underground pipeline is complex, the damage caused by oil leakage should not be underestimated.

In this paper, unmanned aerial vehicles are used to take pictures of oil leakage in oil and gas drilling and ground pipelines. As the situation on the ground is relatively complex, and some buildings and number of buildings are shaded, the segmentation of the collected images poses a great challenge. The fast detection of oil spill method (FD) [79] can detect offshore oil spills and identify vessels that have dumped oil. On the surface of the sea, the background is single and the oil target is obvious. The f-divergence minimization (FDM) [80] can recognize oil spill images with different shapes. This method effectively reduces a large number of labeled data for neural network training. The one dot fuzzy initialization method (ODFI) [81] that the fuzzy connecting between any initial point and the remaining pixels leads to a physically uniform region which is consistent with the minimization of the initial energy. This method can obtain relatively complete oil spill area. The above methods have a good effect on the segmentation of oil spill images, but they also have different disadvantages. FDM and ODFI require training data sets, and only by completing the training of neural network can the segmentation and identification of oil spill be realized. The FD algorithm is simple and easy to implement, but its ability to deal with complex background image segmentation is weak.

Figure 21 is the result of the PRI, BDE, GCE, VoI, and CPU time of each comparison algorithm. As can be seen from the figure, 3DPCNN-HSOA algorithm has the shortest running time and the highest segmentation accuracy. The FD has poor accuracy, but short operation time, the FDM and ODFI have a good segmentation accuracy, but long operation time. Therefore, 3DPCNN-HSOA algorithm has a good segmentation effect and excellent ability to solve the problem of oil and gas drilling oil leakage and pipeline oil leakage.

Because the ground background is complex and there are many buildings and trees, the algorithm is easy to divide the background of the building into oil pollution areas. The algorithm proposed in this paper has a good ability to segment simple background, as shown in the oil pollution image in Figure 16d, with few tree shadows. The 3DPCNN-HSOA model can best obtain the oil pollution area. However, when the shadow area of trees is large, it is easy to divide the shadow into the dirty oil area. In the future research, we will focus on this problem to improve the segmentation ability of the algorithm and enhance the optimizing ability of the optimization algorithm. At the same time, we will study infrared and satellite image segmentation, to better solve the over-segmentation phenomenon.
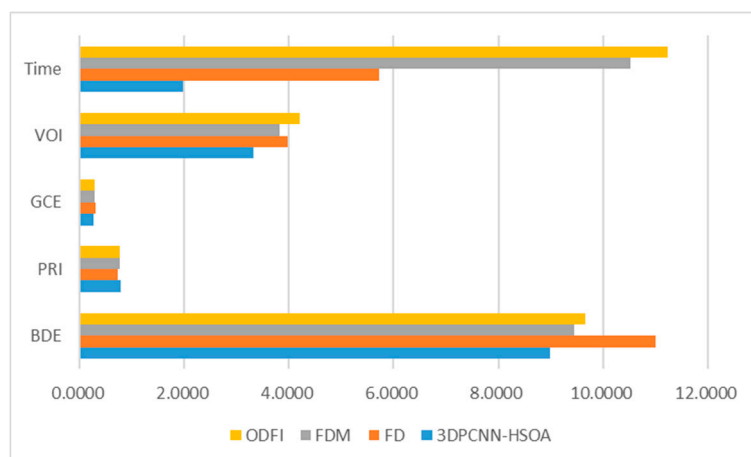
Figure 21. Bar graph of the results of each comparison algorithm.

7. Conclusions

In this paper, HSOA algorithm is adopted to optimize the parameter of the 3DPCNN model, and the ICE is used as the fitness function. We combine the SOA algorithm and the TEO algorithm to improve SOA algorithm, increase the random step size of the algorithm, and improve the optimization ability of the algorithm. This algorithm is compared with other optimization algorithms to jointly optimize 3DPCNN model in satellite image segmentation experiments. As can be seen from PSNR and FSIM values, the 3DPCNN-HSOA model has the highest segmentation accuracy. Finally, we compare the 3DPCNN-HSOA method with the novel image segmentation algorithm, and conduct segmentation experiments on oil pollution images. It can be seen from PRI, VoI, GCE, BDE and CPU time indexes that HSOA's optimization ability to 3DPCNN model is better than the other image segmentation algorithm. Therefore, the 3DPCNN-HSOA algorithm proposed in this paper has better image segmentation accuracy and less CPU time. It has excellent ability to solve the problem of oil pollution image segmentation and can obtain the complete oil pollution area.

Author Contributions: H.J. and Z.X. contributed to the idea of this paper; Z.X. and W.S. performed the experiments; Z.X. wrote the paper; H.J. contributed to the revision of this paper.

Conflicts of Interest: The authors declare no conflict of interest.

References

1. Margarit, G. NEREIDS: New Concepts in Maritime Surveillance for Consolidating Operational Developments. In Proceedings of the 2012 Esa's Seasar Workshop, Tromso, Norway, 18–22 June 2012.
2. Stasolla, M.; Santamaria, C.; Mallorqui, J.J.; Margarit, G.; Walker, N. Automatic ship detection in SAR satellite images: Performance assessment. In Proceedings of the Geoscience and Remote Sensing Symposium, Milan, Italy, 26–31 July 2015.
3. Fingas, M.F.; Brown, C.E. Review of oil spill remote sensing. *Mar. Pollut. Bull.* **2014**, *83*, 9–23. [CrossRef] [PubMed]
4. Alves, T.M.; Kokinou, E.; Zodiatis, G.; Lardener, R.; Panaqiotakis, C.; Radhakrishnan, H. Modelling of oil spills in confined maritime basins: The case for early response in the Eastern Mediterranean Sea. *Environ. Pollut.* **2015**, *206*, 390–399. [CrossRef] [PubMed]
5. Alves, T.M.; Kokinou, E.; Zodiatis, G.; Radhakrishnan, H.; Panaqiotakis, C.; Lardner, R. Multidisciplinary oil spill modeling to protect coastal communities and the environment of the Eastern Mediterranean Sea. *Sci. Rep.* **2016**, *6*, 36882.

6. Hazen, E.L.; Carlisle, A.B.; Wilson, S.G.; Ganong, J.E.; Castleton, M.R.; Schallet, R.J.; Stokesbury, M.J.W.; Bograd, S.J.; Block, B.A. Quantifying overlap between the Deepwater Horizon oil spill and predicted bluefin tuna spawning habitat in the Gulf of Mexico. *Sci. Rep.* **2016**, *6*, 33824. [CrossRef] [PubMed]

7. Ge, J.; Shi, L.; Wang, Y.C.; Zhao, H.Y.; Yao, H.B.; Zhu, Y.B.; Zhang, Y.; Zhu, H.W.; Wu, H.A.; Yu, S.H. Joule-heated graphene-wrapped sponge enables fast clean-up of viscous crude-oil spill. *Nat. Nanotechnol.* **2017**, *12*, 434. [CrossRef] [PubMed]

8. Mera, D.; Canedo, V.; Cotos, J.M.; Betanzos, A.A. On the use of feature selection to improve the detection of sea oil spills in SAR images. *Comput. Geosci.* **2017**, *100*, 166–178. [CrossRef]

9. Chamoso, P.; Perez, A.; Rodriguez, S.; Corchado, J.M.; Sempere, M.; Rizo, R.; Aznar, F.; Pujol, M. Modeling Oil-Spill Detection with multirotor systems based on multi-agent systems. In Proceedings of the International Conference on Information Fusion, Salamanca, Spain, 7–10 July 2014.

10. Brekke, C.; Solberg, A.H.S. Oil spill detection by satellite remote sensing. *Remote Sens. Environ.* **2005**, *95*, 1–13. [CrossRef]

11. Oribayo, O.; Feng, X.; Rempel, G.L.; Pan, Q. Synthesis of lignin-based polyurethane/graphene oxide foam and its application as an absorbent for oil spill clean-ups and recovery. *Chem. Eng. J.* **2017**, *323*, 191–202. [CrossRef]

12. Evans, M.; Liu, J.; Bacosa, H.; Rosenheim, B.E.; Liu, Z. Petroleum hydrocarbon persistence following the Deepwater Horizon oil spill as a function of shoreline energy. *Mar. Pollut. Bull.* **2017**, *115*, 47–56. [CrossRef]

13. Zhang, C.; Xie, Y.C.; Liu, D.; Wang, L. Fast Threshold image segmentation based on 2D Fuzzy Fisher and Random Local Optimized QPSO. *IEEE Trans. Image Process.* **2017**, *26*, 1355–1362. [CrossRef]

14. Li, Y.; Jiao, L.; Shang, R.; Stolkin, S. Dynamic-context cooperative quantum-behaved particle swarm optimization based on multilevel thresholding applied to medical image segmentation. *Inf. Sci.* **2015**, *294*, 408–422. [CrossRef]

15. Aja-Fernández, S.; Curiale, A.H.; Vegas-Sánchez-Ferrero, G. A local fuzzy thresholding methodology for multiregion image segmentation. *Knowl. Based Syst.* **2015**, *83*, 1–12. [CrossRef]

16. Mostafa, A.; Vavadi, H.; Uddin, K.M.S.; Zhou, Q. Diffuse optical tomography using semiautomated coregistered ultrasound measurements. *J. Biomed. Opt.* **2017**, *22*, 1. [CrossRef] [PubMed]

17. Lee, H.S.; Kang, K. Simultaneous Traffic Sign Detection and Boundary Estimation Using Convolutional Neural Network. *IEEE Trans. Intell. Transp. Syst.* **2018**, *19*, 1652–1663. [CrossRef]

18. Muniraj, I.; Guo, C.; Malallah, R.; Maraka, H.V.R.; Ryle, J.P.; Sheridan, J.T. Subpixel based defocused points removal in photon-limited volumetric dataset. *Opt. Commun.* **2017**, *387*, 196–201. [CrossRef]

19. Liu, Z.; Watson, J.; Allen, A. Efficient Image Preprocessing of Digital Holograms of Marine Plankton. *IEEE J. Ocean. Eng.* **2017**, *43*, 83–92. [CrossRef]

20. Chen, L.; Fan, L.; Xie, G.; Huang, K. Moving-Object Detection From Consecutive Stereo Pairs Using Slanted Plane Smoothing. *IEEE Trans. Intell. Transp. Syst.* **2017**, *18*, 3093–3102. [CrossRef]

21. Tan, K.S.; Isa, N.A.M. Color Image Segmentation Using Histogram Thresholding Fuzzy C-Means Hybrid Approach. *Pattern Recognit.* **2011**, *44*, 1–15.

22. Li, Y.; Kim, J. An unconditionally stable hybrid method for image segmentation. *Appl. Numer. Math.* **2014**, *82*, 32–43. [CrossRef]

23. Johnson, J.L.; Padgett, M.L. PCNN models and applications. *IEEE Trans. Neural Netw.* **1999**, *10*, 480. [CrossRef]

24. Lücken, L.; Ronsin, D.P.; Worlitzer, V.M.; Yanchuk, S. Pattern reverberation in networks of excitable systems with connection delays. *Chaos* **2017**, *27*, 013114.

25. Storath, M.; Rickert, D.; Unser, M.; Weinmann, A. Fast Segmentation From Blurred Data in 3D Fluorescence Microscopy. *IEEE Trans. Image Process.* **2017**, *26*, 4856–4870. [CrossRef]

26. Xiang, R. Image segmentation for whole tomato plant recognition at night. *Comput. Electron. Agric.* **2018**, *154*, 434–442. [CrossRef]

27. Chen, Y.; Ma, Y.; Kim, D.; Park, S. Region-Based Object Recognition by Color Segmentation Using a Simplified PCNN. *IEEE Trans. Neural Netw. Learn. Syst.* **2015**, *26*, 1682–1697. [CrossRef]

28. Li, H.; Guo, L.; Yu, P.; Chen, J.; Tang, Y. Image segmentation based on Iterative Self-organizing Data Clustering threshold of PCNN. In Proceedings of the IEEE International Conference on Cloud Computing and Internet of Things, Dalian, China, 2 March 2017.

29. He, F.; Guo, Y.; Gao, C. An improved pulse coupled neural network with spectral residual for infrared pedestrian segmentation. *Infrared Phys. Technol.* **2017**, *87*, 22–30. [CrossRef]

30. Jing, L.; Shi, B.; Li, M.; Nan, Z.; Ma, Y. An automatic segmentation method of a parameter-adaptive PCNN for medical images. *Int. J. Comput. Assist. Radiol. Surg.* **2017**, *12*, 1511–1519.

31. Gao, H.Y.; Su, X.; Liang, Y.S. Automatic Image Segmentation Using PCNN and Quantum Geese Swarm Optimization. In Proceedings of the International Conference in Communications Springer, Singapore, 7 June 2018.

32. Bai, W.; Zhang, W.; Zhou, N.; Tang, L.; Ma, C.; Shi, X. Transmission line voltage classes identification based on particle swarm optimization algorithm and PCNN. *Ferroelectrics* **2017**, *521*, 6–17. [CrossRef]

33. Ruder, S. An overview of gradient descent optimization algorithms. *arXiv* **2016**, arXiv:1609.04747.

34. Fei, Z.; Li, B.; Yang, S.; Xing, C. A Survey of Multi-Objective Optimization in Wireless Sensor Networks: Metrics, Algorithms and Open Problems. *IEEE Commun. Surv. Tutor.* **2016**, *19*, 550–586. [CrossRef]

35. Yang, X.S.; Gandomi, A.H. Bat algorithm: A novel approach for global engineering optimization. *Eng. Comput.* **2012**, *29*, 464–483. [CrossRef]

36. Chakri, A.; Khelif, R.; Benouaret, M.; Yang, X.S. New directional bat algorithm for continuous optimization problems. *Expert Syst. Appl.* **2017**, *69*, 159–175. [CrossRef]

37. Cheng, M.Y.; Prayogo, D. Symbiotic Organisms Search: A new metaheuristic optimization algorithm. *Comput. Struct.* **2014**, *139*, 98–112. [CrossRef]

38. Vincent, F.Y.; Redi, A.A.N.P.; Yang, C.L.; Ruskartina, E.; Santosa, B. Symbiotic organism search and two solution representations for solving the capacitated vehicle routing problem. *Appl. Soft Comput.* **2017**, *52*, 657–672.

39. Mirjalili, S.; Lewis, A. The Whale Optimization Algorithm. *Adv. Eng. Softw.* **2016**, *95*, 51–67. [CrossRef]

40. Mehne, H.H.; Mirjalili, S. A Parallel Numerical Method for Solving Optimal Control Problems based on Whale Optimization Algorithm. *Knowl. Based Syst.* **2018**, *151*, 114–123. [CrossRef]

41. Saremi, S.; Mirjalili, S.; Lewis, A. Grasshopper Optimisation Algorithm: Theory and application. *Adv. Eng. Softw.* **2017**, *105*, 30–47. [CrossRef]

42. Mirjalili, S.Z.; Mirjalili, S.; Saremi, S.; Faris, H.; Aljarah, I. Grasshopper optimization algorithm for multi-objective optimization problems. *Appl. Intell.* **2018**, *48*, 805–820. [CrossRef]

43. Wu, J.; Wang, H.; Li, N.; Yao, P.; Huang, Y.; Su, Z.; Yu, Y. Distributed trajectory optimization for multiple solar-powered UAVs target tracking in urban environment by Adaptive Grasshopper Optimisation Algorithm. *Aerosp. Sci. Technol.* **2017**, *70*, 497–510. [CrossRef]

44. Kaveh, A.; Dadras, A. A novel meta-heuristic optimization algorithm: Thermal exchange optimization. *Adv. Eng. Softw.* **2017**, *110*, 69–84. [CrossRef]

45. Dhiman, G.; Kumar, V. Seagull optimization algorithm: Theory and its applications for large-scale industrial engineering problems. *Knowl. Based Syst.* **2019**, *165*, 169–196. [CrossRef]

46. Ewees, A.A.; Elaziz, M.A.; Houssein, E.H. Improved Grasshopper Optimization Algorithm using Opposition-based Learning. *Expert Syst. Appl.* **2018**, *112*, 156–174. [CrossRef]

47. Yan, B.; Zhao, Z.; Zhou, Y.; Yuan, W. A particle swarm optimization algorithm with random learning mechanism and Levy flight for optimization of atomic clusters. *Comput. Phys. Commun.* **2017**, *219*, 76–86. [CrossRef]

48. Moradi, M.H.; Foroutan, V.B.; Abedini, M. Power flow analysis in islanded Micro-Grids via modeling different operational modes of DGs: A review and a new approach. *Renew. Sustain. Energy Rev.* **2017**, *69*, 248–262. [CrossRef]

49. Tizhoosh, H.R. Opposition-Based Learning: A New Scheme for Machine Intelligence. In Proceedings of the International Conference on Computational Intelligence for Modelling, Control and Automation, and International Conference on Intelligent Agents, Web Technologies and Internet Commerce, Vienna, Austria, 28–30 November 2005.

50. Trivedi, I.N.; Kumar, A.; Ranpariya, A.H.; Jangir, P. Economic Load Dispatch problem with ramp rate limits and prohibited operating zones solve using Levy flight Moth-Flame optimizer. In Proceedings of the IEEE International Conference on Energy Efficient Technologies for Sustainability (ICEETS), Nagercoil, India, 7–8 April 2016.

51. Chenhua, X.U.; Chengxian, L.I.; Xin, Y.U.; Huang, Q.B. Improved grey wolf optimization algorithm based on chaotic Cat mapping and Gaussian mutation. *Comput. Eng. Appl.* **2017**, *53*, 1–9.

52. Liu, B.; Grout, V.; Nikolaeva, A. Efficient Global Optimization of Actuator Based on a Surrogate Model Assisted Hybrid Algorithm. *IEEE Trans. Ind. Electron.* **2018**, *65*, 5712–5721. [CrossRef]

53. Yang, Y.; Yang, B.; Niu, M. Adaptive infinite impulse response system identification using opposition based hybrid coral reefs optimization algorithm. *Appl. Intell.* **2018**, *48*, 1689–1706. [CrossRef]

54. Guangqian, D.; Bekhrad, K.; Azarikhah, P.; Maleki, A. A hybrid algorithm based optimization on modeling of grid independent biodiesel-based hybrid solar/wind systems. *Renew. Energy* **2018**, *122*, 551–560. [CrossRef]

55. Alsaeedan, W.; Menai, M.E.B.; Al-Ahmadi, S. A Hybrid Genetic-Ant Colony Optimization Algorithm for the Word Sense Disambiguation Problem. *Inf. Sci.* **2017**, *417*, 20–38. [CrossRef]

56. Aziz, M.A.E.; Ewees, A.A.; Hassanien, A.E. Whale Optimization Algorithm and Moth-Flame Optimization for multilevel thresholding image segmentation. *Expert Syst. Appl.* **2017**, *83*, 242–256. [CrossRef]

57. Singh, K.; Singh, K.; Son, L.H.; Aziz, A. Congestion Control in Wireless Sensor Networks by Hybrid Multi-Objective Optimization Algorithm. *Comput. Netw.* **2018**, *138*, 90–107. [CrossRef]

58. Daniel, E.; Anitha, J.; Gnanaraj, J. Optimum laplacian wavelet mask based medical image using hybrid cuckoo search-grey wolf optimization algorithm. *Knowl. Based Syst.* **2017**, *131*, 58–69. [CrossRef]

59. Orhan, E.; Güçlü, A. A new hybrid ant colony optimization algorithm for solving the no-wait flow shop scheduling problems. *Appl. Soft Comput.* **2018**, *72*, 166–176.

60. Garg, H. A Hybrid PSO-GA Algorithm for Constrained Optimization Problems. *Appl. Math. Comput.* **2016**, *274*, 292–305. [CrossRef]

61. Zhou, D.; Shao, Y. Region growing for image segmentation using an extended PCNN model. *IET Image Process.* **2018**, *12*, 729–737. [CrossRef]

62. Kong, W.; Zhang, L.; Yang, L. Novel fusion method for visible light and infrared images based on NSST–SF–PCNN. *Infrared Phys. Technol.* **2014**, *65*, 103–112. [CrossRef]

63. Ying, L.; Zhou, Y.; Luo, Q. Lévy Flight Trajectory-Based Whale Optimization Algorithm for Global Optimization. *IEEE Access* **2017**, *5*, 6168–6186.

64. Wang, R.; Zhou, Y.; Zhao, C.; Wu, H. A hybrid flower pollination algorithm based modified randomized location for multi-threshold medical image segmentation. *Bio-Med. Mater. Eng.* **2015**, *26* (Suppl. 1), S1345–S1351. [CrossRef] [PubMed]

65. Gao, H.; Pun, C.M.; Kwong, S. An efficient image segmentation method based on a hybrid particle swarm algorithm with learning strategy. *Inf. Sci.* **2016**, *369*, 500–521. [CrossRef]

66. Liang, H.; Liu, H.; Liu, Y.; Shen, Y.; Li, F.; Man, Y. A Hybrid Bat Algorithm for Economic Dispatch with Random Wind Power. *IEEE Trans. Power Syst.* **2018**, *33*, 5052–5061. [CrossRef]

67. Zhong, Y.; Feng, F.; Liu, Y.; Zhao, B.; Jiao, H.; Zhang, L. SatCNN: Satellite image dataset classification using agile convolutional neural networks. *Remote Sens. Lett.* **2017**, *8*, 136–145. [CrossRef]

68. Hu, Y.C.; Chang, C.C. Variable rate vector quantization scheme based on quadtree segmentation. *IEEE Trans. Consum. Electron.* **2002**, *45*, 310–317.

69. Niu, S.; Chen, Q.; Sisternes, L.; Ji, Z.; Zhou, Z.; Rubince, D.L. Robust noise region-based active contour model via local similarity factor for image segmentation. *Pattern Recognit.* **2017**, *61*, 104–119. [CrossRef]

70. Guo, Z.; Kwon, Y.H.; Lee, K.; Wang, K.; Wahle, A.; Alward, W.L.M.; Fingert, J.H.; Bettis, D.I.; Johnson, C.A.; Garvin, M.K.; et al. Optical Coherence Tomography Analysis Based Prediction of Humphrey 24-2 Visual Field Thresholds in Patients with Glaucoma. *Investig. Ophthalmol. Vis. Sci.* **2017**, *58*, 3975–3985. [CrossRef]

71. Ji, S.; Wei, S.; Lu, M. Fully Convolutional Networks for Multisource Building Extraction from an Open Aerial and Satellite Imagery Data Set. *IEEE Trans. Geosci. Remote Sens.* **2018**, *99*, 1–13. [CrossRef]

72. Mdakane, L.W.; Kleynhans, W. An Image-Segmentation-Based Framework to Detect Oil Slicks from Moving Vessels in the Southern African Oceans Using SAR Imagery. *IEEE J. Sel. Top. Appl. Earth Obs. Remote Sens.* **2017**, *10*, 2810–2818. [CrossRef]

73. Helmy, A.K.; El-Taweel, G.S. Image Segmentation Scheme Based on SOM–PCNN in Frequency Domain. *Appl. Soft Comput.* **2016**, *40*, 405–415. [CrossRef]

74. Zhang, K.; Zhang, L.; Lam, K.M.; Zhang, D. A Level Set Approach to Image Segmentation with Intensity Inhomogeneity. *IEEE Trans. Cybern.* **2017**, *46*, 546–557. [CrossRef] [PubMed]

75. Liang, H.; Jia, H.; Xing, Z.; Ma, J.; Peng, X. Modified grasshopper algorithm based multilevel thresholding for color image segmentation. *IEEE Access* **2019**, *7*, 11258–11295. [CrossRef]

76. Pare, S.; Bhandari, A.K.; Kumar, A.; Singh, G.K. An optimal Color Image Multilevel Thresholding Technique using Grey-Level Co-occurrence Matrix. *Expert Syst. Appl.* **2017**, *87*, 335–362. [CrossRef]

77. Sarkar, S.; Das, S.; Chaudhuri, S.S. A multilevel color image thresholding scheme based on minimum cross entropy and differential evolution. *Pattern Recognit. Lett.* **2015**, *54*, 27–35. [CrossRef]

78. Akram, F.; Garcia, M.A.; Puig, D. Active contours driven by local and global fitted image models for image segmentation robust to intensity inhomogeneity. *PLoS ONE* **2017**, *12*, e0174813. [CrossRef] [PubMed]

79. Lupidi, A.; Staglianò, D.; Martorella, M.; Berizzi, F. Fast Detection of Oil Spills and Ships Using SAR Images. *Remote Sens.* **2017**, *9*, 230. [CrossRef]

80. Yu, X.; Zhang, H.; Luo, C.; Qi, H.; Ren, P. Oil Spill Segmentation via Adversarial f-Divergence Learning. *IEEE Trans. Geosci. Remote Sens.* **2018**, *56*, 4973–4988. [CrossRef]

81. Ren, P.; Xu, M.; Yu, Y.; Chen, F.; Jiang, X.; Yang, E. Energy Minimization with One Dot Fuzzy Initialization for Marine Oil Spill Segmentation. *IEEE J. Ocean. Eng.* **2018**, *99*, 1–14. [CrossRef]